IEEE Access
Multidisciplinary | Rapid Review | Open Access Journal

Received April 2, 2019, accepted April 15, 2019, date of publication April 23, 2019, date of current version May 2, 2019.

Digital Object Identifier 10.1109/ACCESS.2019.2912094

A Model Predictive Controller With Switched Tracking Error for Autonomous Vehicle Path Tracking

CHUANYANG SUN[1], XIN ZHANG[1], QUAN ZHOU[1], AND YING TIAN[2]

[1]Beijing Key Laboratory of Powertrain for New Energy Vehicle, School of Mechanical, Electronic, and Control Engineering, Beijing Jiaotong University, Beijing 100044, China

[2]Yangtze River Delta Research Institute, Beijing Jiaotong University, Zhenjiang 212009, China

Corresponding author: Xin Zhang (zhangxin@bjtu.edu.cn)

This work was supported by the National Key Research and Development Program of China under Grant 2016YFB0101000.

ABSTRACT Autonomous vehicle path tracking accuracy and vehicle stability can hardly be accomplished by one fixed control frame in various conditions due to the changing vehicle dynamics. This paper presents a model predictive control (MPC) path-tracking controller with switched tracking error, which reduces the lateral tracking deviation and maintains vehicle stability for both normal and high-speed conditions. The design begins by comparing the performance of three MPC controllers with different tracking error. The analyzing results indicate that in the steady-state condition the controller with the velocity heading deviation as the tracking error significantly improves the tracking accuracy. Meanwhile, in the transient condition, by substituting the steady-state sideslip for real-time sideslip to compute the velocity heading deviation, the tracking overshoot can be reduced. To combine the strengths of these two methods, an MPC controller with switched tracking error is designed to improve the performance in both steady-state and transient conditions. The regime condition of a vehicle maneuver and the switching instant are determined by a fuzzy-logic-based condition classifier. Both normal and aggressive driving scenarios with the vehicle lateral and longitudinal acceleration combination of 5 m/s^2 and 8 m/s^2 are designed to test the proposed controller through CarSim-Simulink platform. The simulation results show the improved performance of the MPC controller with switched tracking error both in tracking accuracy and vehicle stability in both scenarios.

INDEX TERMS Autonomous vehicles, path tracking, predictive control, switched tracking error, condition classifier.

I. INTRODUCTION

Autonomous vehicle technology aims to increase driving safety, reduce traffic congestion and emissions, and improve energy efficiency [1]–[4]. Path tracking is a basic part of the vehicle control module to execute the predefined path from the motion planning layer by determining the desired actuating input to correct tracking errors [5]. To track the path accurately and steadily, the tracking error representation and control algorithms are of vital importance.

Several kinds of tracking errors have been used in the design of path tracking controller. In some simple geometric tracking controllers, such as pure pursuit [6], the steering angle is directly determined from the lateral deviation through the geometrical relationship between the vehicle and the desired path.

For the controllers based on kinematic and dynamic model, an explicit tracking error representation is usually needed to describe the relative position of the vehicle to the desired path. The most extensive tracking error used in the kinematic model based controllers is expressed with the error in longitudinal and lateral directions and orientation error in the global frame [7]–[9]. This method is suitable for robots and low speed vehicles. However, when the speed goes up, the tracking accuracy and vehicle stability of this class of controllers cannot be maintained due to the ignorance of vehicle dynamics.

Several kinds of tracking error representations are used with dynamic vehicle model to realize path tracking at high speed. Yaw rate error and lateral deviation are one of the

The associate editor coordinating the review of this manuscript and approving it for publication was Jianyong Yao.

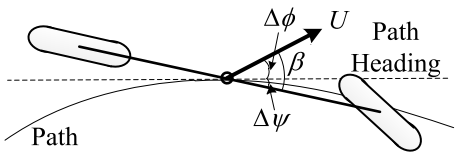

FIGURE 1. Velocity heading deviation and vehicle heading deviation. U is vehicle velocity, β is sideslip, $\Delta\psi$ is the vehicle heading deviation, $\Delta\phi$ is the velocity heading deviation.

popular states to represent tracking error. Multiple approaches are proposed to steer the vehicle yaw rate to the desired reference value to achieve path tracking [10]–[14]. Since the yaw rate is directly related to the vehicle yaw stability, it is easy to keep the vehicle steady through this model. However, the desired reference value is the solution to a kinematic model or a steady-state bicycle model. Using this value as a reference input would ignore the natural transient dynamics of the vehicle [15], [16], which could lead to a poor tracking accuracy in some conditions. Some other states, such as sideslip, steering angle or a combination, are also used as the desired references [15]–[19], and they will face the same problem.

Another common way to formulate the tracking error is utilizing the vehicle heading deviation instead of yaw rate error to maintain the vehicle travel orientation, and controllers based on this tracking error model are designed to force the vehicle heading deviation to zeros [20]–[25]. Chuan Hu etc. References [26], [27] designed a robust controller that can minimize vehicle heading and lateral deviations under disturbances and uncertainties. Brown etc. Reference [28] presented a path tracking controller based on model predictive control (MPC) to minimize the vehicle heading deviation, and the controller could achieve stabilization and obstacle avoidance simultaneously. A simple but effective feedback-feedforward steering controller using vehicle heading deviation as control output was proposed in [29], and the controller could keep a lower complexity and maintain stability even at the handling limits. However, choosing the vehicle heading deviation as a control output may not always minimize the lateral deviation effectively, especially when the sideslip is high, as shown in Figure 1. The vehicle heading deviation and lateral deviation cannot be made to zero at steady-state simultaneously [17], [30].

To eliminate the steady-state tracking error, the vehicle velocity heading deviation, which is the deviation of the vehicle travelling orientation and path heading, as shown in Figure 1, is applied to model the tracking error. Werling *et al.* [31] presented a steering controller that can track the velocity heading and validated the controller through the experiment with a low friction coefficient. Kapania and Gerdes [17] explained that zero steady-state lateral deviation requires the vehicle velocity vector to be tangent to the path, which means the vehicle velocity heading deviation to be zero. But the experiment results show that the designed feedback controller based on the velocity heading deviation would spin out at limits of handling. To maintain the stability margins, the steady-state sideslip instead of real-time sideslip is used in the final controller, and the performance was demonstrated through experiment. Although the vehicle stability is improved by combining steady-state sideslip in the vehicle heading deviation, the tracking accuracy in steady-state condition is not as good as that of using real-time sideslip, which is due to the transient dynamics is ignored when computing the steady-state sideslip.

Variety of control algorithms have been used in path tracking design, including classical algorithms. [32], [33], robust algorithms [34], [35], optimal algorithms [36], [37], etc. Recently, model predictive control (MPC) has become the most attractive method in the control of autonomous vehicles, due to the capability of systematically including system constraints and future predictions in the design procedure, which is perfect for dealing with vehicle stability constraints as well as changing vehicle and tire dynamics [4], [28], [38]–[40]. Besides, the inherent robustness of MPC guarantees the system robustness to some degree [38], [41].

Most of the existing path-tracking controllers are designed based on a fixed tracking error representation. However, in the presence of the changing vehicle dynamics under various conditions, these controllers may not guarantee a high performance in a certain scenario. Inspired by the research in [17], this paper designs a MPC controller that takes the velocity heading deviation as the tracking error, and the real-time sideslip and the steady-state sideslip are switched to compute the velocity heading deviation in the steady-state and transient condition, respectively. A fuzzy-logic based condition classifier is developed to indicate the regime condition and the switching instant. The main contributions of this paper include that: 1) the deficiencies and strengths of using steady-state sideslip and real-time sideslip to compute velocity heading deviation as the tracking error is analyzed, and the necessity of a switched tracking error is clarified; 2) a vehicle condition classifier is constructed based on fuzzy-logic to classify the vehicle maneuver into the steady-state or transient condition; 3) based on the condition classifier, an MPC path tracking controller with switched tracking error is proposed, which is capable of reducing tracking error and maintaining vehicle stability in steady-state and transient conditions, simultaneously.

The configuration of this paper is as follows. The vehicle dynamic model, a linearized tire model and tracking error model are presented in section II. The control problem about using different tracking error as control output is stated in section III. The fuzzy-logic based condition classifier and the detailed MPC path tracking controller with a switched tracking error design are presented in section IV, and simulation is conducted in section V. Finally, Section VI concludes the paper with a brief discussion of the results.

II. DYNAMIC MODELING

A. VEHICLE LATERAL DYNAMIC MODEL

In this paper, a single-track 'bicycle' model including lateral and yaw motion is applied to capture the tracking

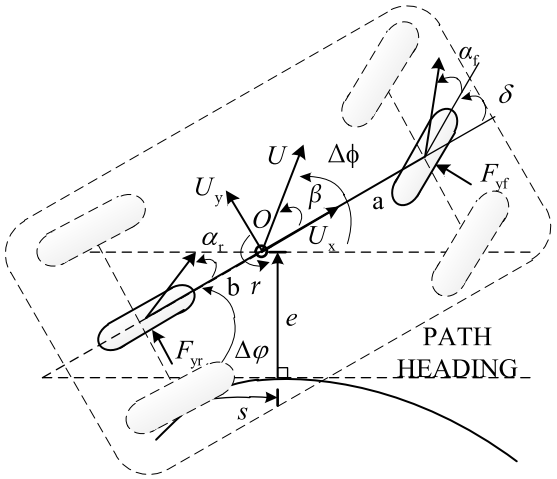

FIGURE 2. Bicycle model schematic.

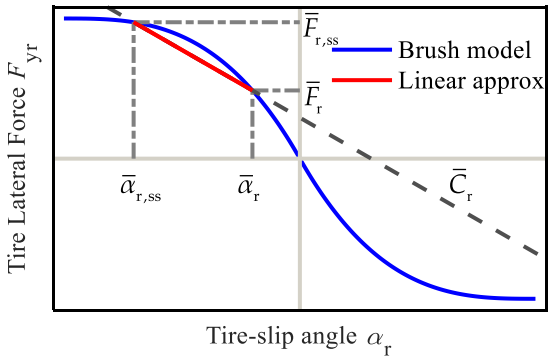

FIGURE 3. The linear approximation of brush tire model. $\bar{\alpha}_r$ is the tire slip angle at time k; $\bar{\alpha}_{r,ss}$ is the assumed steady-state tire slip angle at step N_P over the prediction horizon; $\bar{F}_r$ and $\bar{F}_{r,ss}$ are the corresponding lateral force.

performance and handling stability, shown in Figure 2. The front steering angle δ is the only actuation. To make the optimization problem of δ convex, the longitudinal speed U_x over the prediction horizon is assumed to be constant. Whereas an external speed controller will be used to track the desired speed profile.

Under the constant speed and small angle assumptions and using Newton's theorem, the sideslip angle β and yaw rate r are described by the equations of motion:

$$\dot{\beta} = \frac{F_{yf} + F_{yr}}{mU_x} - r \tag{1}$$

$$\dot{r} = \frac{aF_{yf} - bF_{yr}}{I_{zz}} \tag{2}$$

where m and I_{zz} are the vehicle mass and yaw inertia. $F_{y[f,r]}$ is the lateral tire force of the front and rear axle. a and b is the distance from the center of gravity to the front and rear axles respectively.

B. TIRE MODEL

Neglecting vertical load transfer and using the Fiala brush tire model, the lateral tire force $F_{y[f,r]}$ is modeled as a function of tire slip angle $\alpha_{[f,r]}$:

$$F_{y[f,r]} = f_{\text{tire}}(\alpha) = \begin{cases} -C_\alpha \tan\alpha + \dfrac{C_\alpha^2}{3\mu F_z}|\tan\alpha|\tan\alpha \\ -\dfrac{C_\alpha^3}{27\mu^2 F_z^2}\tan^3\alpha, \quad |\alpha| < \arctan\left(\dfrac{3\mu F_z}{C_\alpha}\right) \\ -\mu F_z sgn\alpha, \qquad \text{otherwise} \end{cases} \tag{3}$$

where μ is the coefficient of friction, F_z is the vertical force, α is the tire slip angle, and C_α is the tire cornering stiffness.

The tire slip angles α_f and α_r, under small angle approximations, can be expressed as:

$$\alpha_f = \beta + \frac{ar}{U_x} - \delta \tag{4}$$

$$\alpha_r = \beta - \frac{br}{U_x} \tag{5}$$

In order to simplify the nonlinearity between tire slip angle and lateral force, and taking the saturation of the tire into account, the front lateral force F_{yf} is considered as the control input of the model [28]. The F_{yf} generated by the MPC optimization can be mapped to the desired δ by

$$\delta = \beta + \frac{ar}{U_x} - f_{\text{tire}}^{-1}(F_{yf}) \tag{6}$$

where $f_{\text{tire}}^{-1}(F_{yf})$ is the inverted tire model, which can calculate the tire slip from tire force through numerical method.

The rear tire force is determined by linearizing Equation (3) through the method proposed in [4]. The method assumes that the tire cornering stiffness keeps constant in the MPC prediction horizon N_P, as shown in Figure 3.

The steady-state solution of rear tire force to Equation (1-2) is expressed as:

$$\bar{F}_{r,ss} = \frac{ma}{L}U_x^2\kappa \tag{7}$$

where κ is the curvature of the desired path at the position of time k.

The equivalent cornering stiffness over prediction horizon can be written as:

$$\bar{C}_r = \frac{(\bar{F}_{r,ss} - \bar{F}_r)}{\bar{\alpha}_{r,ss} - \bar{\alpha}_r}, \quad i = 0, \ldots, N_P - 1 \tag{8}$$

The approximate expression of the predicted rear tire lateral force is:

$$F_{yr}(k+i) = \bar{F}_r - \bar{C}_r(\alpha_r(k+i) - \bar{\alpha}_r), \quad i = 0, \ldots, N_P - 1 \tag{9}$$

where $\alpha_r(k+i)$ is the predicted rear tire slip angle which can be calculated by Equation (5).

C. TRACKING ERROR REPRESENTATION

Using the vehicle's center of gravity as the control reference point, the tracking error between the vehicle and the relative point on the desired path can be represented by two states: lateral deviation e, vehicle heading deviation $\Delta\psi$, as shown in Figure 2. The vehicle heading deviation can be expressed as:

$$\Delta\psi = \psi - \psi_{\mathrm{r}} \tag{10}$$

where ψ is the vehicle heading, ψ_{r} is the heading of the path.

Besides, as mentioned in the introduction, the deviation between the vehicle travelling orientation and the path heading can be represented by the velocity heading deviation, which is yielded as:

$$\Delta\phi = \Delta\psi + \beta \tag{11}$$

Substitute steady-state sideslip β_{ss} for real-time sideslip β, and yield the substituted velocity heading deviation:

$$\Delta\phi_{\mathrm{s}} = \Delta\psi + \beta_{\mathrm{ss}} \tag{12}$$

To make it clear, the substituted velocity heading deviation is not the steady-state velocity heading deviation. In fact, the value of the steady-state velocity heading deviation is zero.

The steady-state sideslip β_{ss} can be obtained from Equation (3), (5) and (7) as:

$$\beta_{\mathrm{ss}} = f_{\mathrm{tire}}^{-1}(F_{\mathrm{yr}}^{\mathrm{ss}}) + b\kappa \tag{13}$$

From Equation (13) above, we can notice that β_{ss} is a function of path curvature κ and vehicle speed U_{x}. Since both κ and U_{x} are known at each sampling instant, β_{ss} can be seen as a priori.

Making the small angle approximation for β and $\Delta\psi$, the derivatives of $\Delta\psi$ and e can be obtained:

$$\Delta\dot{\psi} = r - U_x\kappa \tag{14}$$

$$\dot{e} = U_{\mathrm{x}}(\beta + \Delta\psi) \tag{15}$$

The system state space can be yielded from Equations (1-2) and (10-15) as follows:

$$\dot{\mathbf{x}} = \mathbf{A}_{\mathrm{c}}^{t}\mathbf{x}(t) + \mathbf{B}_{F_{\mathrm{yf}}}^{t}F_{\mathrm{yf}}(t) + \mathbf{B}_{\kappa}^{t}\kappa(t) + \mathbf{d}_{\bar{\alpha}_{\mathrm{r}}}^{t} \tag{16}$$

$$\mathbf{y}_j = \mathbf{C}_j^{t}\mathbf{x} + \mathbf{d}_j^{t}, \quad j = 1, 2, 3. \tag{17}$$

where $\mathbf{x} = \begin{bmatrix}\beta & r & \Delta\psi & e\end{bmatrix}^T$ is the state vector; $\mathbf{y}_1 = \begin{bmatrix}\Delta\psi & e\end{bmatrix}^T$, $\mathbf{y}_2 = \begin{bmatrix}\Delta\phi & e\end{bmatrix}^T$, $\mathbf{y}_3 = \begin{bmatrix}\Delta\phi_{\mathrm{s}} & e\end{bmatrix}^T$ is the tracking error and also as control output; and

$$\mathbf{A}_{\mathrm{c}}^{t} = \begin{bmatrix} \frac{-2\bar{C}_{\mathrm{r}}}{mU_{\mathrm{x}}} & \frac{2\bar{C}_{\mathrm{r}}b}{mU_{\mathrm{x}}^2} - 1 & 0 & 0 \\ \frac{2\bar{C}_{\mathrm{r}}b}{I_{zz}} & -\frac{2\bar{C}_{\mathrm{r}}b^2}{I_{zz}U_{\mathrm{x}}} & 0 & 0 \\ 0 & 1 & 0 & 0 \\ U_{\mathrm{x}} & 0 & U_{\mathrm{x}} & 0 \end{bmatrix}, \quad \mathbf{B}_{F_{\mathrm{yf}}}^{t} = \begin{bmatrix} \frac{2}{mU_{\mathrm{x}}} \\ \frac{2a}{I_{zz}} \\ 0 \\ 0 \end{bmatrix},$$

$$\mathbf{B}_{\kappa}^{t} = \begin{bmatrix} 0 \\ 0 \\ -U_{\mathrm{x}} \\ 0 \end{bmatrix}, \quad \mathbf{d}_{\bar{\alpha}_{\mathrm{r}}}^{t} = \begin{bmatrix} \frac{2(\bar{F}_{\mathrm{r}} + \bar{C}_{\mathrm{r}}\bar{\alpha}_{\mathrm{r}})}{mU_{\mathrm{x}}} \\ -\frac{2b(\bar{F}_{\mathrm{r}} + \bar{C}_{\mathrm{r}}\bar{\alpha}_{\mathrm{r}})}{I_{zz}} \\ 0 \\ 0 \end{bmatrix},$$

$$\mathbf{C}_1^{t} = \begin{bmatrix} 0 & 0 & 1 & 0 \\ 0 & 0 & 0 & 1 \end{bmatrix}, \quad \mathbf{d}_1^{t} = \mathbf{0},$$

$$\mathbf{C}_2^{t} = \begin{bmatrix} 1 & 0 & 1 & 0 \\ 0 & 0 & 0 & 1 \end{bmatrix}, \quad \mathbf{d}_2^{t} = \mathbf{0},$$

$$\mathbf{C}_3^{t} = \mathbf{C}_1^{t}, \quad \mathbf{d}_3^{t} = \begin{bmatrix}\beta_{\mathrm{ss}} & 0\end{bmatrix}^T.$$

Using the zero-order hold discretization method, we can get the discrete system model:

$$\mathbf{x}(k+1) = \mathbf{A}_{\mathrm{c}}\mathbf{x}(k) + \mathbf{B}_{F_{\mathrm{yf}}}F_{\mathrm{yf}}(k) + \mathbf{B}_{\kappa}\kappa(k) + \mathbf{d}_{\bar{\alpha}_{\mathrm{r}}} \tag{18}$$

$$\mathbf{y}_j(k) = \mathbf{C}_j\mathbf{x}(k) + \mathbf{d}_j, \quad j = 1, 2, 3. \tag{19}$$

III. MPC CONTROLLER DESIGN AND TRACKING ERROR COMPARISON

In the design of path tracking controller for autonomous vehicle, the most two important objectives we need to consider are (1) good handling and stability; (2) high tracking accuracy. Given three different kinds of tracking error $\mathbf{y}_j$ ($j = 1, 2, 3.$), now we design the MPC controller and compare the performance of these tracking error.

A. MPC CONTROLLER DESIGN

1) VEHICLE STABILITY CONSTRAINTS

The design of vehicle stability constraints is defined by the bounds of two vital indicators of vehicle stability. Under the assumptions of steady-state cornering and the given tire model, the bounds of β and r reflect the maximum capabilities of the vehicle's tires [28].

The maximum steady-state yaw rate can be expressed as follows:

$$r_{\max} = \frac{g\mu}{U_{\mathrm{x}}} \tag{20}$$

where g is the gravity.

The vehicle sideslip β when the rear tires approach saturation is:

$$\beta_{ss,\max} = \alpha_{r,sat} + \frac{br}{U_{\mathrm{x}}} \tag{21}$$

where

$$\alpha_{\mathrm{r,sat}} = \tan^{-1}(3\frac{mg\mu}{C_{\alpha_{\mathrm{r}}}}\frac{a}{a+b}) \tag{22}$$

The constraints defined by (20) and (21) can be concisely expressed as the inequality:

$$|\mathbf{H}_{\mathrm{v}}\mathbf{x}| \leq \mathbf{G}_{\mathrm{v}} \tag{23}$$

2) MPC FORMULATION

Central to the MPC controller is to solve a convex optimization problem at each time step to find an optimal sequence of

future input:

$$\mathbf{F}_{\mathrm{yf}}(k) = [F_{\mathrm{yf}}^{k}, F_{\mathrm{yf}}^{k+1}, \ldots, F_{\mathrm{yf}}^{k+N_{\mathrm{C}}-1}]^{T} \tag{24}$$

where N_{C} is the control horizon.

For each tracking error $\mathbf{y}_j$ ($j = 1, 2, 3.$), the optimization problem can be formulated as follows:

$$\min_{\mathbf{U}(k)} J_{N_{\mathrm{P}}} = \sum_{i=k}^{k+N_{\mathrm{P}}-1} (\mathbf{y}_j^i)^T \mathbf{Q} \mathbf{y}_j^i + \sum_{i=k}^{k+N_{\mathrm{C}}-1} \Delta F_{\mathrm{yf}}^i R \Delta F_{\mathrm{yf}}^i + \mathbf{W}\varepsilon_{\mathrm{v}} \tag{25}$$

subject to model Equation (18) and (19):

$$\left|\mathbf{H}_{\mathrm{v}}\mathbf{x}^i\right| \leq \mathbf{G}_{\mathrm{v}} + \varepsilon_{\mathrm{v}}, \quad i = k, \ldots, k + N_{\mathrm{C}} - 1 \tag{26}$$

$$\Delta F_{\mathrm{yf}}^i = F_{\mathrm{yf}}^i - F_{\mathrm{yf}}^{i-1}, \quad i = k, \ldots, k + N_{\mathrm{C}} - 1 \tag{27}$$

$$\left|\Delta F_{\mathrm{yf}}^i\right| \leq \Delta F_{\mathrm{yf,max}}, \quad i = k, \ldots, k + N_{\mathrm{C}} - 1 \tag{28}$$

$$\Delta F_{\mathrm{yf}}^i = 0, \quad i = k + N_{\mathrm{C}}, k + N_{\mathrm{C}} + 1, \ldots, k + N_{\mathrm{P}} - 1 \tag{29}$$

$$\left|F_{\mathrm{yf}}^i\right| \leq F_{\mathrm{yf,max}}, \quad i = k, \ldots, k + N_{\mathrm{C}} - 1 \tag{30}$$

where $\mathbf{U}(k) = [\mathbf{F}_{\mathrm{yf}}(k), \varepsilon_{\mathrm{v}}]^T$, and ε_{v} is a non-negative slack variable used to ensure the optimization problem is always feasible. N_{P} is the prediction horizon and $N_{\mathrm{P}} > N_{\mathrm{C}}$, $\mathbf{Q}$, R and $\mathbf{W}$ are weighting matrices of appropriate dimensions. $\Delta F_{\mathrm{yf,max}}$ and $F_{\mathrm{yf,max}}$ are the slew rate capabilities and the maximum lateral force.

The optimal front lateral force input $F_{\mathrm{yf}}^*(k)$ can be obtained through the first element of the optimal solution sequence $\mathbf{U}^*(k)$. The steering angle δ that will be applied to the vehicle could be obtained by mapping from $F_{\mathrm{yf}}^*(k)$ through Equation (6).

In order to accurately capture the propagation of β and r at a high frequency, the sampling time T_{s} is set to be 0.02s. The value of control horizon N_{C}, predictive horizon N_{P} and weighting matrices were obtained through iteratively tuning by the principles mentioned in [42], [43]:

$$N_{\mathrm{C}} = 15, N_{\mathrm{P}} = 50, \quad \mathbf{Q} = \begin{bmatrix} 1000 & 0 \\ 0 & 5 \end{bmatrix}, \; R = 10, \\ \mathbf{W} = \begin{bmatrix} 10 & 10 & 10 & 10 \end{bmatrix} \tag{31}$$

B. TRACKING ERROR COMPARISON

Figure 4 shows results from using the different tracking error $\mathbf{y}_j$ ($j = 1, 2, 3.$) as control output of the MPC controller to track the desired path with a constant curvature $\kappa = 0.02\ \mathrm{m}^{-1}$, given a lateral acceleration of $a_{\mathrm{y}} = 6$ m/s. The initial value of lateral deviation e and heading deviation $\Delta\psi$ are 0.5 m and 0.

It can be seen from Figure 4(a) the path tracking overshoots and steady-state errors of the original controller ($\mathbf{y}_1 = \begin{bmatrix} \Delta\psi & e \end{bmatrix}^T$) are both significant. A comparison of the two ameliorated controllers shows that the controller with β_{ss} ($\mathbf{y}_3 = \begin{bmatrix} \Delta\phi_{\mathrm{s}} & e \end{bmatrix}^T$) has a better performance in the transient

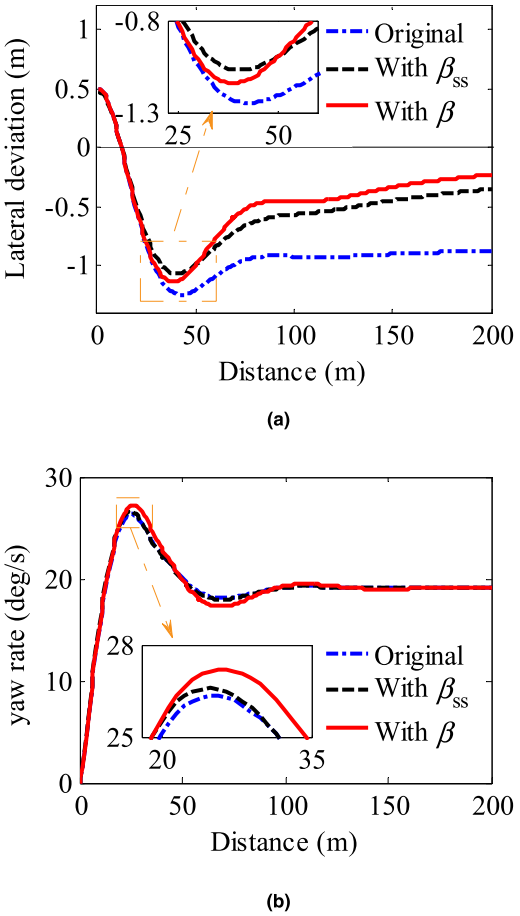

FIGURE 4. Simulation results of MPC controllers with different control output. (a) Lateral deviation. (b) Yaw rate.

response, whereas the controller with β ($\mathbf{y}_2 = \begin{bmatrix} \Delta\phi & e \end{bmatrix}^T$) has the lower static tracking error. The yaw rate responses of the original controller and the controller with β_{ss} are analogous as shown in Figure 4(b). However, the overshoot and oscillation of yaw rate controlled by the controller with β are higher than the other two controllers.

A detailed explanation for the tracking improvement using the velocity heading deviation $\Delta\phi$ instead of the vehicle heading deviation $\Delta\psi$ as the tracking error can be found in [17]. Here we discuss the influence addressed by a different form of sideslip on vehicle maneuvers.

The tracking error $\|\Delta\psi + \beta_{\mathrm{ss}}\|$ and $\|\Delta\psi + \beta\|$ are forced to converge to zero due to the cost function in both MPC controllers. In the first form, the heading deviation $\Delta\psi$ is forced to converge to -β_{ss} as $t \to \infty$, whereas in the second form $\Delta\psi$ is forced to converge to $-\beta$. As β is also a variable, so the desired equilibrium of $\Delta\psi$ is unfixed at a specific time. This is why the yaw rate oscillation of the second controller is higher in the transient condition.

On the other hand, the steady-state value is the desired state response produced by a reference model which is built under the steady-state and zero tracking error assumption. Due to the neglecting of some vehicle travelling and tracking characteristics such as acceleration of the vehicle, lateral deviation,

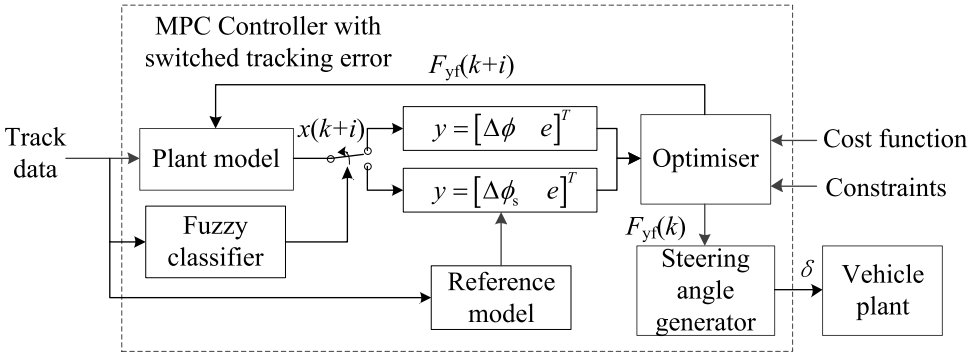

FIGURE 5. The structure of the MPC controller with switched tracking error.

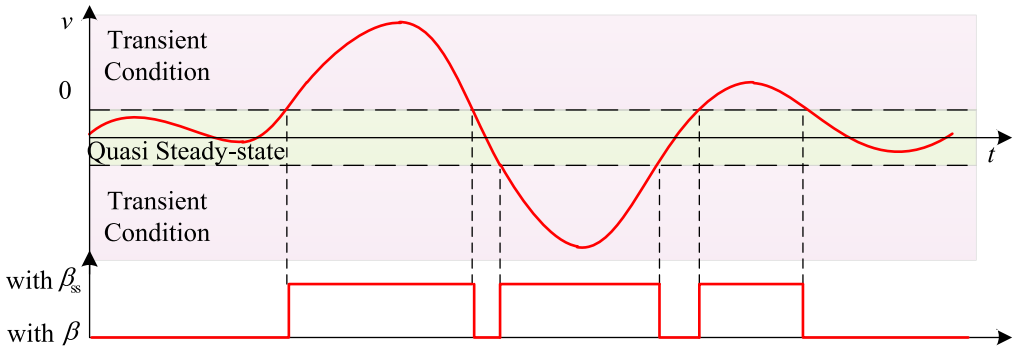

FIGURE 6. The control process of the switched MPC controller.

vertical load transfer and track width, the value produced by the reference model can be significantly different with real-time value. When the vehicle is travelling in the quasi-steady-state or steady-state condition (constant curvature), the static tracking error of the controller with β_{ss} cannot be eliminated due to the difference between the desired value and the real-time value of the side slip.

In order to improve the yaw oscillation and tracking performance in both transient condition and steady-state condition, a controller with switched tracking error should be designed.

IV. DESIGN OF THE MPC CONTROLLER WITH SWITCHED TRACKING ERROR

In section III, the deficiency of taking different tracking error as the control output is analyzed, and the simulation result indicates that a fixed tracking error is not applicable to all conditions. Therefore, in this section, an MPC controller with switched tracking error is constructed by means of switching the tracking error $\mathbf{y} = [\,\Delta\phi \;\; e\,]^T$ and $\mathbf{y} = [\,\Delta\phi_s \;\; e\,]^T$, which will be determined by a fuzzy classifier. The structure of the controller is shown in Figure 5.

Figure 6 shows the control process of the MPC controller with switched tracking error. When the choosing variables are big enough, which indicates the vehicle is travelling in a transient condition, the fuzzy classifier will switch the tracking error to $\mathbf{y} = [\,\Delta\phi_s \;\; e\,]^T$. When the variables converge to the neighborhood of the origin, the vehicle reaches in quasi-steady-state condition, and the controller switches to the tracking error $\mathbf{y} = [\,\Delta\phi \;\; e\,]^T$.

A. CONDITION CLASSIFICATION

The vehicle maneuvers cannot always possible be classified into transient or steady-state conditions clearly and precisely, especially in the intermediate phase [44]. The variables and the limits used to classify the maneuvers can be various due to the various purposes of the classification.

To determine the appropriate variables to characterize the vehicle lateral dynamics generated by transient and steady-state responses, simulation through MATLAB and CarSim are implemented. The desired path used in the simulation is a 2.3 km CarSim default path with a wide range of curvature. The controller with β and controller with β_{ss} proposed in section III are used respectively, and both of the controllers track the entire path at a lateral acceleration of 5m/s^2, 6m/s^2, 7m/s^2, 8m/s^2, 9m/s^2 once. The root-mean-square (RMS) values for vehicle states are computed to capture the nature of the vehicle maneuvers.

Yaw acceleration $\dot{r}$, lateral jerk J, velocity heading deviation $\Delta\phi$ and the rate of change of velocity heading deviation $\Delta\dot{\phi}$ are chosen as the condition classification variables. The variations in lateral dynamics generated by vehicle acceleration/braking meanwhile cornering can be reflected

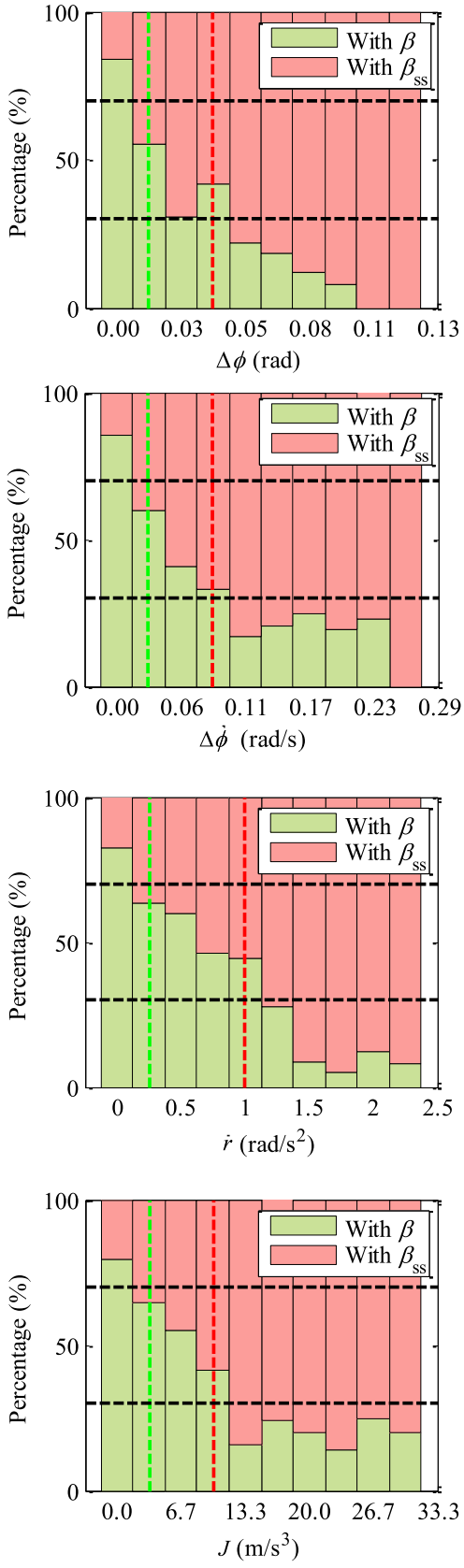

FIGURE 7. The better performance points percentage contrast of two controllers in different segments.

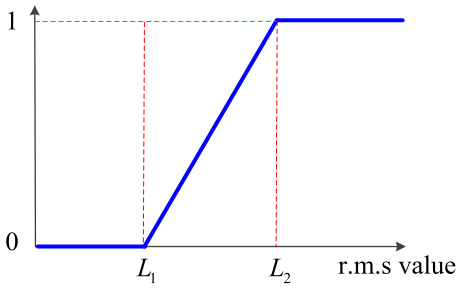

FIGURE 8. The membership function for the fuzzy-logic algorithm.

in the RMS value of lateral jerk and yaw acceleration. The RMS value of velocity heading deviation and the rate of change of velocity heading deviation can provide the information concerning the dynamics variation in advance, which is caused by the changing path curvature with respect to the influence of the changing speed.

The interval between zero and the maximum of the RMS value of each variable $[0, \max(v_i)]$ is divided into 10 equal segments of width Δv_i ($i = 1, 2, 3, 4$ corresponding to $\dot{r}$, J, $\Delta\phi$, $\Delta\dot{\phi}$). We compare the lateral tracking deviation of two controllers at the same position of the desired path in corresponding cases and obtain all the points with better tracking performance. Based on the distribution of these points, the percentage of each controller in every segment of each variable is calculated, as shown in Figure 7.

Figure 7 shows that the increased RMS value leads to a higher percentage of the controller with β_{ss} for all the variables, providing feasibility for classifying vehicle conditions. As an example, when the RMS value for yaw acceleration is lower than Δv_1, the majority points (more than 70%) are conducted by controller with β, indicating a steady-state condition; beyond $4\Delta v_1$ the majority points are conducted by controller with β_{ss}, and the variation of lateral jerk is considered large enough to produce a transient maneuver. Between Δv_1 and $4\Delta v_1$ the performance of two controllers is close, and it is assumed to be an intermediate condition. The limits to divide the RMS values into three phases for other variables can be obtained using the same criterion.

A fuzzy-logic algorithm with trapezoidal fuzzification function is employed to handle the non-deterministic nature of the intermediate phase, as shown in Figure 8. A membership degree in range 0-1 is determined to classify a maneuver. The values of L_1 and L_2 are obtained from the analysis above, as reported in table 1. Below L_1 (membership function $= 0$) the maneuver is considered completely stationary; beyond L_2 (membership function $= 1$) the maneuver is considered fully transient; between L_1 and L_2, the membership degree linearly passes from 0 to 1.

A 'condition indicator' α is computed as a weighted mean of the membership degree of four variables to indicate the condition, as shown in Figure 9. Table 1 lists the weights of four variables. The signal of velocity heading deviation

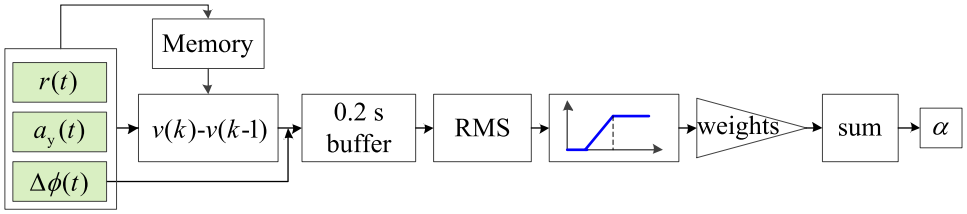

FIGURE 9. Fuzzy-logic scheme to determine the condition indicator.

TABLE 1. The limits of rate of change and weights of variables for condition classification.

Variables	Symbol	L1	L2	Weights
Yaw acceleration	$\dot{r}$	0.25 rad/s2	1 rad/s2	0.2
Lateral jerk	J	3.33 m/s3	10 m/s3	0.2
Velocity heading deviation	$\Delta\phi$	0.013 rad	0.04 rad	0.3
Rate of change of velocity heading deviation	$\Delta\dot{\phi}$	0.03 rad/s	0.08 rad/s	0.3

TABLE 2. Parameter values of the vehicle and path.

Parameter	Symbol	Value	Units
Vehicle mass	m	1230	kg
Yaw inertia	I_{zz}	1343.1	kg·m^2
Front axle-O distance	a	1.04	m
Rear axle-O distance	b	1.56	m
Front cornering stiffness	C_{α_f}	48,840	N/rad
Rear cornering stiffness	C_{α_r}	32,887	N/rad
Friction coefficient	μ	0.95	n/a

and its rate of change is directly related to the tracking error and can provide information around both vehicle dynamics and path curvature, and the weight is sensibly higher. To characterize the vehicle dynamics properly and avoid high-frequency switching, the buffer time T_b for condition classifier is set as 0.2 s, as the frequency of vehicle dynamics is about 7 Hz [44].

B. MPC CONTROLLER WITH SWITCHED TRACKING ERROR

With the classifier of the vehicle condition, the MPC controller with switched tracking error based on the Equation (25-30) can be formulated as follows:

1) For time k, check the condition of the vehicle.
   if $n < 10$ (T_b/T_s)
   set $n = n + 1$;
   set $\alpha(k) = \alpha(k\text{-}1)$;
   else
   update $\alpha(k)$ using the algorithm in Figure 9;
   set $n = 0$;
   end.
2) Optimization: Find the optimal $\mathbf{U}(k)$, such that the following optimization problem is solved:

$$\min_{\mathbf{U}(k)} J_{N_P}(\mathbf{y}, \mathbf{U}(k)) \tag{32}$$

subject to Equation (18-19), (26-30), and

$$\mathbf{y}^i = \left[\, \Delta\phi^i \;\; e^i \,\right]^T, \quad i = k, \ldots, k + N_P - 1 \text{ for } \alpha(k) < 0.5,$$
$$\mathbf{y}^i = \left[\, \Delta\phi_s^i \;\; e^i \,\right]^T, \quad i = k, \ldots, k + N_P - 1 \text{ for } \alpha(k) \geq 0.5.$$

3) Receding horizon control

$$F_{yf}^*(k) = \left[\, 1 \;\; 0 \;\ldots\; 0 \,\right] \mathbf{U}^*(k) \tag{33}$$

Calculate the steering angle δ from $F_{yf}^*(k)$ through Equation (6), and apply to the vehicle.
4) Set $k = k + 1$, and update system states, input, output and state-space equations (18).

Repeat steps 1)-4) until k reaches its predefined value.

V. SIMULATION AND RESULTS

In order to verify the effectiveness of the proposed controller, simulation is conducted via MATLAB/Simulink and CarSim, which includes a validated high-fidelity full-vehicle dynamics model. The parameters of the vehicle and path are listed in Table 2.

The desired path for the vehicle to track is a 1.5 km racing road designed by the method proposed in [45] and the path is parameterized as a curvature profile that varies with distance along the path, as shown in Figure 10. The curvature varies between -0.014 m^{-1} and 0.025 m^{-1}. Four different controllers are compared: the original controller ($\mathbf{y}_1 = \left[\, \Delta\psi \;\; e \,\right]^T$), the controller with β($\mathbf{y}_3 = \left[\, \Delta\phi \;\; e \,\right]^T$), the controller with β_{ss} ($\mathbf{y}_3 = \left[\, \Delta\phi_s \;\; e \,\right]^T$), and the proposed controller with switched tracking error developed in section IV is to be tested.

Normal driving and aggressive driving scenarios are discussed in this part. The lateral and longitudinal acceleration combination $\mathbf{a_c}$ is often used as the criteria of driving style and comfort, which can be obtained by:

$$a_c = \sqrt{a_x^2 + a_y^2} \tag{34}$$

where a_x and a_y is the longitudinal and lateral acceleration, respectively.

Generally, when driving speed goes up, the human drivers will reduce a_c to attain comforts [46], [47]. However, a_c is

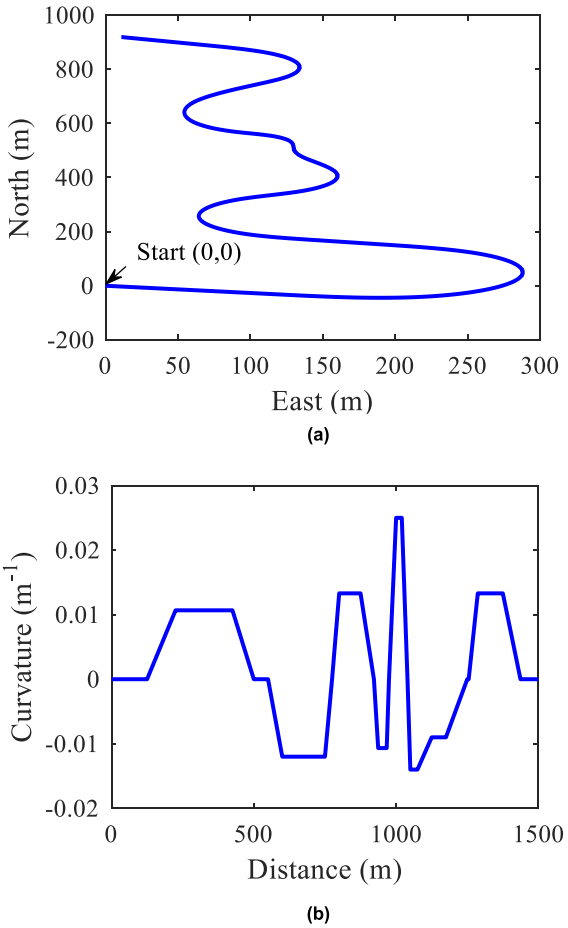

FIGURE 10. The desired path for tracking control test. (a) Overhead plot of the desired path. (b) Curvature as a function of distance along the path.

TABLE 3. Comparison of control results of different controllers.

Data (unit)	symbol	max. (m)	RMS dev. (m)	std. yr. (rad/s)
Normal driving	Original	0.27	0.12	0.10
	With β	0.22	0.06	0.10
	With β_{ss}	0.23	0.07	0.09
	Switched	0.21	0.06	0.09
Aggressive driving	Original	2.76	0.68	0.16
	With β	0.78	0.17	0.15
	With β_{ss}	0.49	0.13	0.13
	Switched	0.49	0.11	0.13

assumed to be constant for each scenario in this paper. This does not make it less convincing, since a specified upper value of a_c for each scenario is used to generate the speed profile [46], [47]. The value of a_c for normal/aggressive driving is set as 5/8 m/s^2, and the peak longitudinal deceleration is -5/-8 m/s^2 and peak lateral acceleration is 5/8 m/s^2. The desired speed profile U_{xd} is generated based on the curvature of the predefined path by the optimal method proposed in [48], which considers the jerk-limits and travel time in the cost function, and the result is shown in Figure 11. The speed

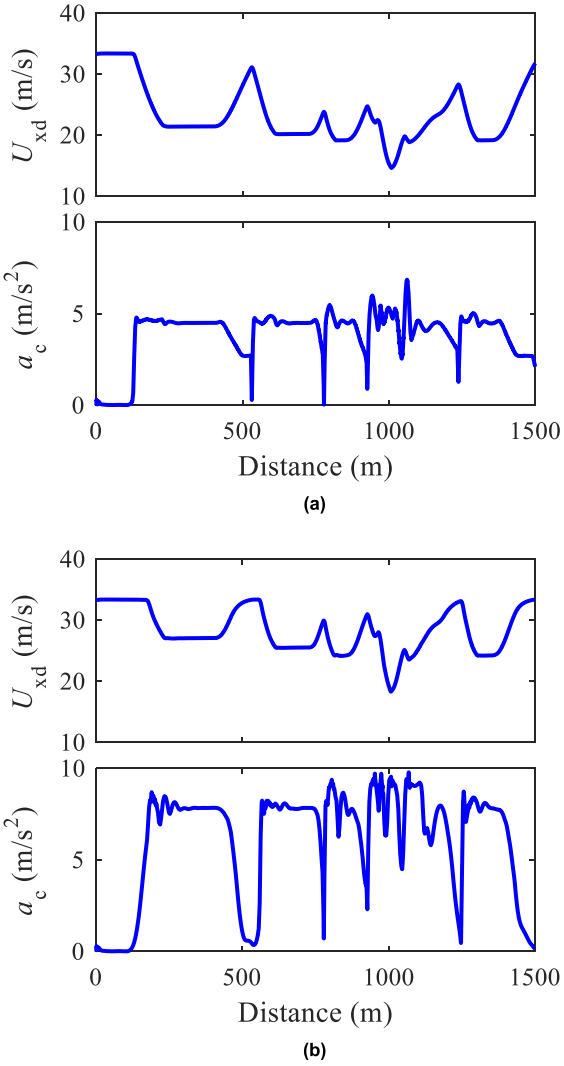

FIGURE 11. Velocity profile and the generated lateral and longitudinal acceleration combination profile. (a) Normal driving. (b) Aggressive driving.

tracking is achieved by a PID longitudinal controller, which is decoupled from the lateral control to reduce the complexity. The same longitudinal controller and stability bounds are used for all cases.

Figure 12 shows the simulation results for both scenarios; the upper part of the figure presents the tracking deviation of all compared controllers. The lower part of Figure 12 shows the value of the condition indicator α calculated from the logic described above and the switch flag ($\alpha < 0.5$, switch flag $= 0$; $\alpha(k) \geq 0.5$, switch flag $= 1$) is also reported. Figure 13 shows the results of condition classification variables.

As shown in Figure 12, for both scenarios, the lateral tracking deviations of the original controller are significantly larger than that of the controllers using $\Delta\phi/\Delta\phi_s$ as a tracking error. This matches the predicted result that taking the vehicle heading deviation as tracking error in the controller cannot minimize the lateral deviation effectively.

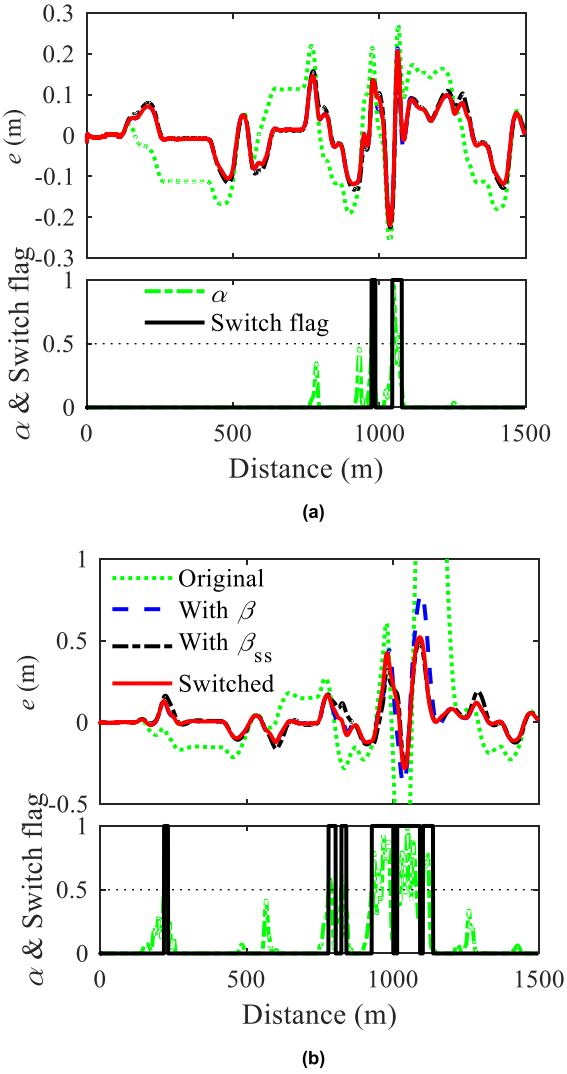

FIGURE 12. Lateral tracking deviation of different controllers, the condition indicator and switch flag of switched MPC controller. (a) Normal driving. (b) Aggressive driving.

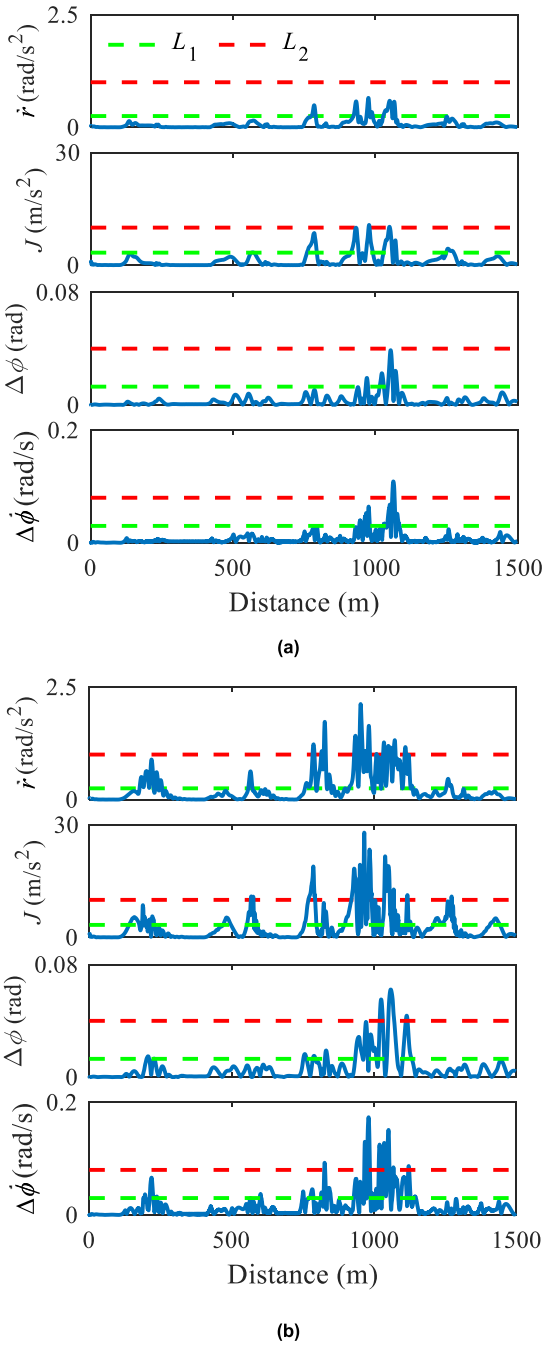

FIGURE 13. Simulation results of the condition classification variables. (a) Normal driving. (b) Aggressive driving.

Figure 12 and Figure 13 show that at most of the normal driving scenario and the aggressive driving scenario, the condition classification variables are under L_1 leading to a small α, which indicates that the vehicle is travelling at quasi-steady-state or fully steady-state condition. The control output of the proposed controller remains as $\mathbf{y} = \begin{bmatrix} \Delta\phi & e \end{bmatrix}^T$ and the switch flag remains at 0. The tracking deviation of the proposed controller and the controller with β remains the same and is smaller than that of the controller with β_{ss}. This matches the predicted result in section III. Using real-time and predicted sideslip to calculate velocity heading deviation in control output, the tracking performance will be improved in quasi-steady-state condition.

At around s = 1000 meters along the track in aggressive driving scenario, all variables reach over L_1, and even over L_2 as shown in Figure 13 due to the sharply changing road curvature. As a result, α reaches over 0.5, indicating the vehicle enters a transient condition. The proposed controller switches the control output to the tracking error $\mathbf{y} = \begin{bmatrix} \Delta\phi_s & e \end{bmatrix}^T$ and the switch flag is set to 1. As we can see from Figure 12, at this condition all the controllers still can remain stable, but the tracking deviation of the controller with β becomes significantly larger than the other two controllers with β_{ss} in their control output. The proposed controller follows the curve of the controller with β_{ss} closely, which indicates that the designed condition indicator can identify the vehicle maneuvers clearly and precisely.

As the tracking results summarized in Table 3 shows, the designed MPC controller with switched tracking error can reduce the tracking deviation RMS value, while maintaining a lower deviation maximum and yaw oscillation simultaneously in both scenarios.

VI. CONCLUSION

A MPC path tracking controller that can minimize the tracking deviation and maintain vehicle stability simultaneously for autonomous vehicle in a wide range of conditions is designed by utilizing the benefits of switched tracking error. By comparing the performance of the controller with different tracking error, velocity heading deviation is chosen as the tracking error. The steady-state sideslip and real-time sideslip are switched to compute the velocity heading deviation to combine strength of each in terms of vehicle condition. The variables and its limits used to indicate the vehicle condition are determined in terms of statistics, and a condition classifier based on fuzzy-logic is constructed to classify a vehicle maneuver into steady-state or transient condition. Simulation results in both normal driving and aggressive driving scenarios show that the proposed MPC controller with switched tracking error can track the desired path accurately and steadily in both steady-state and transient condition. One potential drawback of this controller is that the ability to reject external disturbances and model uncertainties is not ensured. Future work will seek to use robust MPC method to improve the robustness of the system and conduct real-time experiment.

REFERENCES

[1] M. Wei, S. Wang, J. Zheng, and D. Chen, "UGV navigation optimization aided by reinforcement learning-based path tracking," *IEEE Access*, vol. 6, pp. 57814–57825, Sep. 2018.

[2] B. Zhang, C. Zong, G. Chen, and B. Zhang, "Electrical vehicle path tracking based model predictive control with a laguerre function and exponential weight," *IEEE Access*, vol. 7, pp. 17082–17097, Jan. 2019.

[3] M. Montazeri-Gh and M. Mahmoodi-K, "Optimized predictive energy management of plug-in hybrid electric vehicle based on traffic condition," *J. Cleaner Prod.*, vol. 139, pp. 935–948, Dec. 2016.

[4] C. Sun, X. Zhang, L. Xi, and Y. Tian, "Design of a path-tracking steering controller for autonomous vehicles," *Energies*, vol. 11, no. 6, p. 1451, Jun. 2018.

[5] B. Paden, M. Čáp, S. Z. Yong, D. Yershov, and E. Frazzoli, "A survey of motion planning and control techniques for self-driving urban vehicles," *IEEE Trans. Intell. Veh.*, vol. 1, no. 1, pp. 33–55, Mar. 2016.

[6] O. Amidi and C. E. Thorpe, "Integrated mobile robot control," *Mobile Robots*, vol. 1388, pp. 504–524, Mar. 1991.

[7] H. Fang, R. Fan, B. Thuilot, and P. Martinet, "Trajectory tracking control of farm vehicles in presence of sliding," *Robot. Auto. Syst.*, vol. 54, no. 10, pp. 828–839, Oct. 2006.

[8] J. P. Timings and D. J. Cole, "Minimum maneuver time calculation using convex optimization," *J. Dyn. Syst., Meas., Control*, vol. 135, no. 3, Mar. 2013, Art. no. 031015.

[9] R. Lenain, B. Thuilot, C. Cariou, and P. Martinet, "Mixed kinematic and dynamic sideslip angle observer for accurate control of fast off-road mobile robots," *J. Field Robot.*, vol. 27, no. 2, pp. 181–196, Mar./Apr. 2010.

[10] J. Wang, J. Steiber, and B. Surampudi, "Autonomous ground vehicle control system for high-speed and safe operation," in *Proc. ACC*, Seattle, WA, USA, Jun. 2008, pp. 218–223.

[11] J. Wang, W. Chen, and T. Wang, "Vision guided intelligent vehicle lateral control based on desired yaw rate," *J. Mech. Eng.*, vol. 48, no. 4, pp. 108–115, Apr. 2012.

[12] D. V. T. Truong and W. Tomaske, "Active front steering system using adaptive sliding mode control," in *Proc. CCDC*, Guiyang, China, May 2013, pp. 253–258.

[13] C. Zhang, J. Hu, J. Qiu, W. Yang, H. Sun, and Q. Chen, "A novel fuzzy observer-based steering control approach for path tracking in autonomous vehicles," *IEEE Trans. Fuzzy Syst.*, vol. 27, no. 2, pp. 278–290, Feb. 2019. doi: 10.1109/TFUZZ.2018.2856187.

[14] A. A. Janbakhsh, M. K. Bayani, and R. Kazemi, "Simultaneous vehicle-handling and path-tracking improvement using adaptive dynamic surface control via a steer-by-wire system," *Proc. Inst. Mech. Eng. D, J. Auto. Eng.*, vol. 227, no. 3, pp. 345–360, Aug. 2013.

[15] S. Mammar and D. Koenig, "Vehicle handling improvement by active steering," *Veh. Syst. Dyn.*, vol. 38, no. 3, pp. 211–242, Sep. 2000.

[16] G. Tagne, R. Talj, and A. Charara, "Design and comparison of robust nonlinear controllers for the lateral dynamics of intelligent vehicles," *IEEE Trans. Intell. Transp.*, vol. 17, no. 3, pp. 796–809, Mar. 2016.

[17] N. R. Kapania and J. C. Gerdes, "Design of a feedback-feedforward steering controller for accurate path tracking and stability at the limits of handling," *Veh. Syst. Dyn.*, vol. 53, no. 12, pp. 1687–1704, Dec. 2015.

[18] J. Guo, Y. Luo, K. Li, and Y. Dai, "Coordinated path-following and direct yaw-moment control of autonomous electric vehicles with sideslip angle estimation," *Mech. Syst. Signal Process.*, vol. 105, pp. 183–199, May 2018.

[19] C. Fu, R. Hoseinnezhad, A. Bab-Hadiashar, and R. N. Jazar, "Direct yaw moment control for electric and hybrid vehicles with independent motors," *Int. J. Vehicle Des.*, vol. 69, nos. 1–4, pp. 1–24 2015.

[20] J. Guldner, V. I. Utkin, and J. Ackermann, "A sliding mode control approach to automatic car steering," in *Proc. ACC*, Baltimore, MD, USA, Jun./Jul. 1993, pp. 1969–1973.

[21] N. Tavan, M. Tavan, and R. Hosseini, "An optimal integrated longitudinal and lateral dynamic controller development for vehicle path tracking," *Latin Amer. J. Solids Struct.*, vol. 12, no. 6, pp. 1006–1023, Jun. 2015.

[22] M. Xin and M. A. Minor, "Backstepping variable structure control of slip-based kinematics and dynamics for improved AGV cornering performance," in *Proc. ICRA*, Hong Kong, May/Jun. 2014, pp. 5286–5291.

[23] N. R. Kapania and J. C. Gerdes, "Path tracking of highly dynamic autonomous vehicle trajectories via iterative learning control," in *Proc. ACC*, Chicago, IL, USA, Jul. 2015, pp. 2753–2758.

[24] B. Mashadi, M. Mahmoodi-K, A. H. Kakaee, and R. Hosseini, "Vehicle path following control in the presence of driver inputs," *Proc. Inst. Mech. Eng. K, J. Multi-Body Dyn.*, vol. 227, no. 2, pp. 115–132, 2013.

[25] B. Mashadi, M. Mahmoudi-Kaleybar, P. Ahmadizadeh, and A. Oveisi, "A path-following driver/vehicle model with optimized lateral dynamic controller," *Latin Amer. J. Solids Struct.*, vol. 11, no. 4, pp. 613–630, Aug. 2014.

[26] C. Hu, H. Jing, R. Wang, F. Yan, and M. Chadli, "Robust H_∞ output-feedback control for path following of autonomous ground vehicles," *Mech. Syst. Signal Process.*, vols. 70–71, pp. 414–427, Mar. 2016.

[27] K. Kritayakirana and J. C. Gerdes, "Autonomous vehicle control at the limits of handling," *Int. J. Veh. Auton. Syst.*, vol. 10, no. 4, pp. 271–296, Jun. 2012.

[28] M. Brown, J. Funke, S. Erlien, and J. C. Gerdes, "Safe driving envelopes for path tracking in autonomous vehicles," *Control Eng. Pract.*, vol. 61, pp. 307–316, Apr. 2017.

[29] K. Kritayakirana and J. C. Gerdes, "Using the centre of percussion to design a steering controller for an autonomous race car," *Vehicle Syst. Dyn.*, vol. 50, pp. 33–51, Jul. 2012.

[30] R. Rajamani, *Vehicle Dynamics and Control*, 2nd ed. Boston, MA, USA: Springer, 2012, pp. 58–60.

[31] M. Werling, P. Reinisch, and L. Gröll, "Robust power-slide control for a production vehicle," *Int. J. Veh. Auton. Syst.*, vol. 13, no. 1, pp. 27–42, 2015.

[32] S. Hima, S. Glaser, A. Chaibet, and B. Vanholme, "Controller design for trajectory tracking of autonomous passenger vehicles," in *Proc. 14th Int. IEEE Conf. Intell. Trans.*, Washington, DC, USA, Oct. 2011, pp. 1459–1464.

[33] D. M. Flickinger and M. A. Minor, "Remote low frequency state feedback kinematic motion control for mobile robot trajectory tracking," in *Proc. IEEE Int. Conf. Robot. Automat.*, Roma, Italy, Apr. 2007, pp. 3502–3507.

[34] H. Aithal and S. Janardhanan, "Trajectory tracking of two wheeled mobile robot using higher order sliding mode control," in *Proc. IEEE ICCCCM*, Allahabad, India, Aug. 2013, pp. 1–4.

[35] X. Li, Z. Wang, J. Zhu, and Q. Chen, "Adaptive tracking control for wheeled mobile robots with unknown skidding," in *Proc. IEEE CCA*, Sydney, NSW, Australia, Sep. 2015, pp. 1674–1679.
[36] C. Hu, R. Wang, F. Yan, and N. Chen, "Should the desired heading in path following of autonomous vehicles be the tangent direction of the desired path?" *IEEE Trans. Intell. Trans. Syst.*, vol. 16, no. 6, pp. 3084–3094, Dec. 2015.
[37] X. Wu, P. Lou, D. Tang, and J. Yu, "An intelligent-optimal predictive controller for path tracking of vision-based automated guided vehicle," in *Proc. IEEE Int. Conf. Inf. Autom.*, Changsha, China, Jun. 2008, pp. 844–849.
[38] J. B. Rawlings and D. Q. Mayne, *Model Predictive Control Theory and Design*, 4th ed. Madison, WI, USA: Nob Hill, 2014, pp. 198–199.
[39] J. Yao and W. Deng, "Active disturbance rejection adaptive control of hydraulic servo systems," *IEEE Trans. Ind. Electron.*, vol. 64, no. 10, pp. 8023–8032, Oct. 2017.
[40] J. Yao, Z. Jiao, and D. Ma, "A practical nonlinear adaptive control of hydraulic servomechanisms with periodic-like disturbances," *IEEE/ASME Trans. Mechatronics*, vol. 20, no. 6, pp. 2752–2760, Dec. 2015.
[41] D. Q. Mayne, J. B. Rawlings, C. V. Rao, and P. O. M. Scokaert, "Constrained model predictive control: Stability and optimality," *Automatica*, vol. 36, no. 6, pp. 789–814, 2000.
[42] S. Bolognani, S. Bolognani, L. Peretti, and M. Zigliotto, "Design and implementation of model predictive control for electrical motor drives," *IEEE Trans. Ind. Electron.*, vol. 56, no. 6, pp. 1925–1936, Jun. 2009.
[43] L. Wang, *Model Predictive Control System Design and Implementation Using MATLAB*. London, U.K.: Springer, 2009, pp. 170–179.
[44] F. Cheli, E. Sabbioni, M. Pesce, and S. Melzi, "A methodology for vehicle sideslip angle identification: Comparison with experimental data," *Veh. Syst. Dyn.*, vol. 45, no. 6, pp. 549–563, May 2007.
[45] X. Li, Z. Sun, D. Cao, D. Liu, and H. He, "Development of a new integrated local trajectory planning and tracking control framework for autonomous ground vehicles," *Mech. Syst. Signal Process.*, vol. 87, pp. 118–137, Mar. 2017.
[46] J. Wang, K. K. Dixon, H. Li, and J. Ogle, "Normal acceleration behavior of passenger vehicles starting from rest at all-way stop-controlled intersections," *Trans. Res. Rec.*, vol. 1883, no. 1, pp. 158–166, Jan. 2004.
[47] G. Reymond, A. Kemeny, J. Droulez, and A. Berthoz, "Role of lateral acceleration in curve driving: Driver model and experiments on a real vehicle and a driving simulator," *Hum. Factors*, vol. 43, no. 3, pp. 483–495, Sep. 2001.
[48] J. A. Matute, M. Marcano, A. Zubizarreta, and J. Perez, "Longitudinal model predictive control with comfortable speed planner," in *Proc. IEEE ICARSC*, Apr. 2018, pp. 60–64.

CHUANYANG SUN was born in Rizhao, China. He received the B.S. degree in mechanical engineering from Beijing Jiaotong University, Beijing, China, in 2014, where he is currently pursuing the Ph.D. degree in mechanical engineering. His current research interests include vehicle dynamics, predictive control, and intelligent vehicle path tracking.

XIN ZHANG received the B.S. degree in mechanical engineering from Zhejiang University, Hangzhou, China, in 1982, the M.S. degree in mechaincal engineering from Xi'an Jiaotong University, Xi'an, China, in 1986, and the Ph.D. degree in mechanical engineering from Beijing Jiaotong University, Beijing, China, in 2000, where she is currently a Professor with the School of Mechanical Engineering. Her current research interests include automobile electronic control, vehicle operation engineering, and intelligent vehicle.

QUAN ZHOU received the B.S. and M.S. degrees in mechanical engineering from Beijing Jiaotong University, in 2004 and 2007, respectively, where he is currently pursuing the Ph.D. degree in mechanical engineering. His current research interests include vehicle dynamics and automobile electronic control.

YING TIAN received the Ph.D. degree in marine engineering from Harbin Engineering University, Harbin, China, in 2002. She was an Academic Visitor with The Ohio State University, USA, in 2013. She is currently an Associate Professor with the School of Mechanical Engineering, Beijing Jiaotong University, China. Her current research interests include automobile electronic control and intelligent vehicle.